Received: 29 June 2022 | Revised: 16 August 2022 | Accepted: 17 August 2022

DOI: 10.1002/pol.20220366

RESEARCH ARTICLE

JOURNAL OF POLYMER SCIENCE WILEY

Conformation control of triplet state diffusion in platinum containing polyfluorene copolymers

Nikol T. Lambeva[1,2] | **Claudius C. Mullen**[1] | **Xuyu Gao**[3] | **Qingjing Wu**[3] | **Robert A. Taylor**[1] | **Youtian Tao**[3] | **Donal D. C. Bradley**[1,4,5]

[1]Department of Physics, University of Oxford, Oxford, UK

[2]Institute of Ion Beam Physics and Materials Research, Helmholtz-Zentrum Dresden-Rossendorf, Dresden, Germany

[3]Key Lab for Flexible Electronics and Institute of Advanced Materials, Nanjing Tech University, Nanjing, P. R. China

[4]Physical Science and Engineering Division, King Abdullah University of Science and Technology (KAUST), Thuwal, Saudi Arabia

[5]NEOM Education Research and Innovation Foundation and NEOM University, Gayal, Tabuk Province, KSA 49643, Saudi Arabia

Correspondence
Nikol T. Lambeva and Donal D. C. Bradley, Department of Physics, University of Oxford, Parks Road, Oxford OX1 3PU, UK.
Email: nikol.lambeva@physics.ox.ac.uk and donal.bradley@neom.com

Funding information
King Abdullah University of Science and Technology; Oxford University; UK Engineering and Physical Sciences Research Council, Grant/Award Number: 1734270; Jiangsu Province Double Creation Team funding program

Abstract

The spectral diffusion of singlet and triplet excitons in 9,9-dioctylfluorene-based conjugated copolymers is investigated using photoluminescence spectroscopy at both low (5 K) and room temperature (300 K). Inclusion of a *N*,*N*-diphenyl-4-(pyridin-2-yl)aniline moiety into the polymer backbone allows subsequent cyclometalation with platinum acetylacetonate to increase the spin-orbit coupling and yield radiative decay from the triplet state. For suitably low fractions (≤5%) of bulky ligand inclusion, cyclometalated or not, the resulting longer sequences of fluorene units are able to adopt the chain-extended β-phase conformation. Comparison between the phosphorescence spectral diffusion in glassy- and β-phase Pt-copolymer samples provide insight into the triplet exciton transfer in more- or less-disordered conjugated polymer films. It is found in the glassy-phase samples with shorter conjugation lengths that the triplet exciton relaxation becomes frustrated at low temperature due to a freezing out of the thermally activated hops required to move from one conjugated segment to another. In contrast, for films containing β-phase chain segments, with increased conjugation lengths, this frustration is lifted as more hopping sites remain accessible through intra-segment motion. This work demonstrates controlled use of changes in molecular conformation to optimize triplet diffusion properties in a member of the widely deployed fluorene-based conjugated copolymers.

KEYWORDS

chain conformations, polyfluorenes, spectral diffusion, triplet state, β-phase

1 | INTRODUCTION

Triplet states play a vital role in the operation of organic semiconductor devices and can strongly affect their performance. For example, light emitting diode (LED) efficiency is determined by the fraction of injected electrons and holes that recombine to form an emissive state. Since the triplet state in regular conjugated polymers is generally weakly emissive due to its spin-forbidden transition to the ground singlet state, this places a limit on device efficiency. LEDs harvesting triplet emission using a combination of organometallic complexes and organic molecules as the

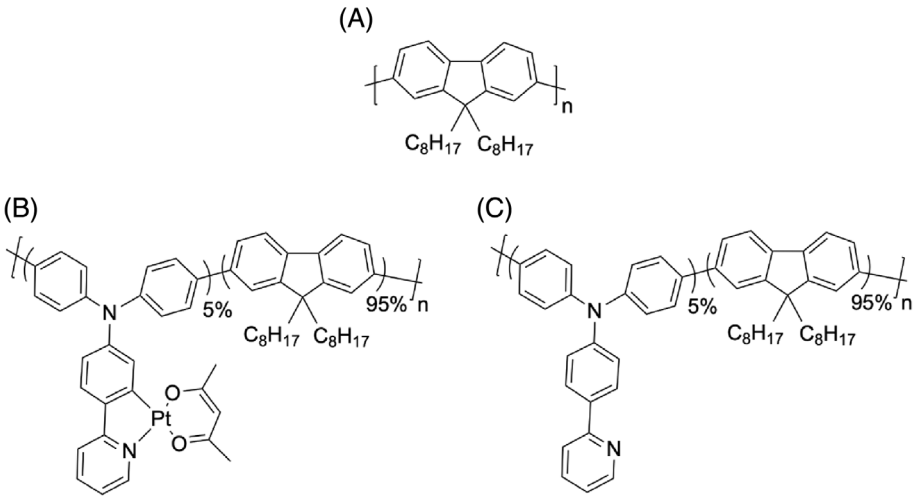

FIGURE 1 Chemical structures of (A) PFO (B) 95F8:5PyTPA-Pt(acac) and (C) 95F8:5PyTPA.

emission layer have gained interest in recent years.[1–3] However, triplet diffusion leading to triplet-charge annihilation and triplet-triplet annihilation (TTA) can lead to efficiency roll-off at high current densities in phosphorescent LEDs.[4–6] Triplet diffusion is also critical for structures based on TTA-induced delayed fluorescence for nonresonant up-conversion of low energy incident red light into high energy blue emission.[7–9] Further development of the material parameters that govern triplet diffusion is consequently desirable for the systematic advancement of these and other applications.

In the current work, the added effect of chain conformation on triplet state diffusion in conjugated copolymer thin films is investigated. Recent literature studying the influence of conformation on triplet states in organic semiconductors has mainly concentrated on the relationship between molecular conformation and degree of spin-orbit coupling. It has been demonstrated for a number of donor-acceptor materials that a twisted conformation leads to reduced singlet-triplet energy gap and considerable increase in intersystem crossing rates.[10–12] However, the effect of chain conformation on triplet diffusion has been largely unexplored. The chain conformation controls the effective conjugation length allowing a transition between more- and less-disordered film structures, corresponding to shorter and longer conjugation lengths.

The material system considered here is a new platinum containing fluorene-based copolymer, in which a small amount of *N*,*N*-diphenyl-4-(pyridin-2-yl)aniline platinum acetylacetonate (PyTPA-Pt(acac)) is inserted into the backbone of the widely-studied poly(9,9-dioctylfluorene) (PFO) blue light emitting polymer (Figure 1A).[13–15] The presence of heavy platinum atoms increases the spin-orbit coupling strength, leading to radiative decay from the triplet state. The PyTPA-Pt(acac) moieties are embedded at mol fractions between 0.5% and 5%.

The loading range selected was guided by prior studies[16,17] that showed successful β-phase formation for 9,9-dioctylfluorene-based copolymers in the presence of bulky co-monomer units for fractions below about 20% and with an eye to avoiding a switch from co-monomer-modulated 9,9-dioctylfluorene emission to co-monomer-dominated emission. The general study of absorption and photoluminescence (PL) emission for (100-X)F8:XPyTPA-Pt(acac) polymer films with different PyTPA-Pt(acac) fractions and 9,9-dioctylfluorene conformations (see Supporting Information Figure S1 to S3 for full data sets) was followed by a more detailed study of triplet energy transfer as a function of temperature and conformation for the 5% loading, 95F8:5PyTPA-Pt(acac) copolymer (Figure 1B). In addition, for reference, we have also characterized (see Figure S1 to S3) the absorption and PL of the corresponding copolymers, (100-X)F8:XPyTPA, that contain the same fractions of the co-monomer *N*,*N*-diphenyl-4-(pyridin-2-yl)aniline (PyTPA), omitting the Pt(acac) units of the cyclometalated version; the chemical structure of the 95F8:5PyTPA polymer is shown in Figure 1C.

For thin film samples, PFO chain segments can adopt glassy- and β-phase structures with chain conformations characterized by different torsion angles between the constituent molecular units. The glassy-phase is a disordered conformation with a broad distribution of inter-monomer torsion angles that averages close to 135°.[18] In contrast, the β-phase conformation is an ordered chain-extended geometry with a torsion angle of ~180° between adjacent fluorene units.[19] The latter conformation leads to a coplanar backbone with the octyl side chains of neighboring monomers positioned on alternating sides of the chain.[18,19] β-phase samples combine a fraction of these chain-extended segments embedded within an otherwise glassy matrix. The formation of planar β-phase segments in PFO is readily evidenced by the appearance of red-shifted, characteristically well-resolved, vibronically-structured absorption and PL emission bands, with a small Stokes' shift between them.[15,20–22] Induction of the β-phase conformation can be achieved either by

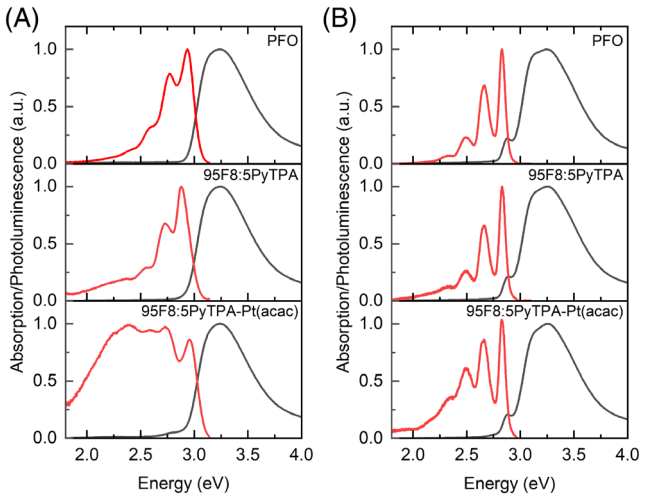

FIGURE 2 Room temperature absorption (right, black line) and photoluminescence (left, red line) spectra for (A) glassy- and (B) β-phase films of PFO, 95F8:5PyTPA and 95F8:5PyTPA-Pt(acac).

(1) slowing down the kinetics of film formation using poor/high boiling point solvents or solution additives[22,23] or (2) via postdeposition exposure to solvent liquid ("solvent flooding")[24,25] or vapor ("solvent annealing").[26,27]

The same processes can be used to generate β-phase segments in (100-X)F8:XPyTPA-Pt(acac) and (100-X)F8:XPyTPA and the resulting absorption and PL spectral changes were characterized, with reference to PFO. Temperature-dependent PL spectroscopy has then also been used to study the spectral diffusion for both singlet and triplet excitons in 95F8:5PyTPA-Pt(acac), a single material system for which we can vary the energetic disorder/conjugation length simply via tuning molecular conformation. This allows demonstration of the ability to optimize triplet diffusion properties through tuning physical structure at the molecular level, without a need for chemical modification.

2 | RESULTS AND DISCUSSION

Figure 2 shows room temperature (RT) absorption and PL spectra for both glassy- (Figure 2A) and β-phase (Figure 2B) films of PFO, 95F8:5PyTPA and 95F8:5PyTPA-Pt(acac). These data confirm the ability to controllably form (and also avoid forming) the β-phase conformation in the longer 9,9-dioctylfluorene segments, with the clear appearance of a characteristic red-edge absorption peak at 2.86 eV (434 nm)[21] in the solvent vapor annealed samples. This peak is absent from the hot-spun glassy films, mirroring the situation for PFO. The PL spectra also show the expected red-shift and enhanced vibronic structure for the β-phase samples, again mirroring the situation for PFO. The PFO and 95F8:5PyTPA spectra are very similar, bar a small red-shift ($\Delta\lambda \approx 8$ nm) in the glassy 95F8:5PyTPA PL spectrum peaks and a slightly stronger long wavelength PL tail. The 95F8:5PyTPA-Pt(acac) copolymer, however, shows weak absorption close to 2.8 eV (443 nm) for both glassy- and β-phase films and the glassy-phase PL spectrum is no longer dominated by 9,9-dioctylfluorene structured vibrational emission, with a competing longer wavelength, largely unstructured contribution of similar magnitude also present. This effect is less evident for the β-phase PL spectra as was also the case for 95F8:5PyTPA.

The 2.8 eV (443 nm) absorption in the 95F8:5PyTPA-Pt(acac) copolymer is characteristic of a metal–ligand charge transfer transition[28] and is evident in the solution and solid-state spectra for the monomeric PyTPA-Pt(acac) unit (Figure S4). It is correspondingly absent from the spectra for the PyTPA monomer, which has its lowest π—π^* solid-state absorption peak at ~3.5 eV (Figure S4). The PL emission from PyTPA monomer films lies in the spectral range of the long wavelength PL tail as also does that for films of the monomeric PyTPA-Pt(acac) unit (Figure S4). The changes in spectra also grow with increasing loading of the PyTPA and PyTPA-Pt(acac) units (Figure S1 and S2). The copolymer spectra are therefore consistent with a loading-weighted combination of 9,9-dioctylfluorene- and co-monomer-centered contributions, where, with the exception of the highest PyTPA-Pt(acac) loadings, the spectra are very much dominated by the former.

Inclusion of the PyTPA and PyTPA-Pt(acac) units causes a strong decrease in RT PL quantum efficiency (PLQE) relative to PFO, especially for the 95F8:5PyTPA-Pt(acac) films, with a more modest decrease for the 95F8:5PyTPA films. Table S1 in Supporting Information provides the PLQE values for both glassy- and β-phase films of all of the different PyTPA and PyTPA-Pt(acac) copolymer fractions and for PFO. The PFO values are fully consistent with literature reports.[13,15,21] Several factors may play a role in this behavior. First, the PyTPA moiety is expected to have notable charge transfer character due to its electron donating triarylamine and electron accepting pyridyl moieties. Second, cyclometallation with Pt(acac) will cause an increase in intersystem crossing from singlet to triplet states and at RT and in air these triplet states will not have a significant emission efficiency. The observed variation with PyTPA and PyTPA-Pt(acac) loading indicates competition between the strong singlet emission centered on 9,9-dioctylfluorene segments and transfer to and limited emission from co-monomer units. The PLQE difference between glassy- and β-phase films then suggests a less favorable transfer regime in the β-phase case.

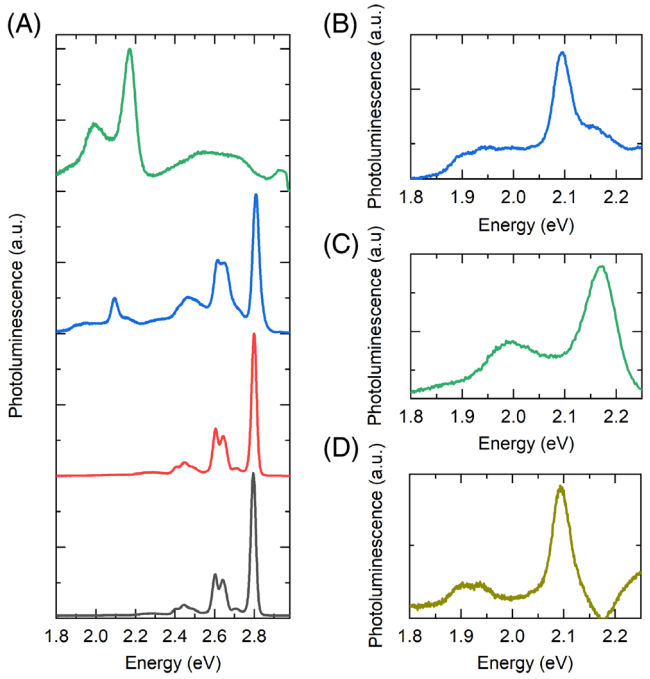

FIGURE 3 (A) Peak normalized PL spectra at 5 K for (from bottom to top) β-phase PFO (black line), β-phase 95F8:5PyTPA (red line), β-phase 95F8:5PyTPA-Pt(acac) (blue line) and glassy-phase 95F8:5PyTPA-Pt(acac) (green line). Also shown are expanded scale triplet PL emission spectra for (B) β-phase 95F8:5PyTPA-Pt(acac) (blue line) and (C) glassy-phase 95F8:5PyTPA-Pt(acac) (green line) films. Comparison of these spectra suggests that the β-phase 95F8:5PyTPA-Pt(acac) spectrum contains a fraction of glassy-phase triplet PL. the difference spectrum (D) (sage line) following subtraction of a weighted glassy-phase spectrum (C) from the β-phase 95F8:5PyTPA-Pt(acac) spectrum (B) reveals the "pure" β-phase triplet PL.

This situation evolves on cooling to low temperature as shown in Figure 3 and Supporting Information. Figure 3A shows (from bottom to top) the 5 K PL spectra for β-phase films of PFO, 95F8:5PyTPA and 95F8:5PyTPA-Pt(acac) and for a glassy film of 95F8:5PyTPA-Pt(acac). A full set of spectra for each sample taken from 300 K to 25 K, at 25 K intervals, is shown together with these 5 K spectra in Figure S5 to S8. The spectral changes for β-phase PFO are as previously reported, with (1) a greatly enhanced resolution of the vibronic peaks that reveals three distinct vibrational modes coupled to the $S_1 \rightarrow S_0$ electronic transition and (2) a major strengthening of the 0–0 peak at 2.8 eV (443 nm) to become the dominant component in the emission, consistent with a reduction in the associated Huang-Rhys parameter.[14] This peak also has a very small Stokes' shift from the associated 2.86 eV $S_0 \rightarrow S_1$ 0–0 absorption peak, consistent with the rigid, chain-extended β-phase conformation. Very similar behavior is seen for the β-phase 95F8:5PyTPA film, also with a reduction in the long wavelength PL tail, showing that the copolymer emission is even more dominated by the 9,9-dioctylfluorene segments at low temperature, with no evidence for significant emission from the PyTPA moieties. As expected, prompt triplet PL emission is not observed for either of these polymers.

In comparison, the 95F8:5PyTPA-Pt(acac) films show a broader range of spectral changes. At 5 K the glassy-phase films show an even more suppressed singlet PL emission component than at RT (Figure 3A). The β-phase 95F8:5PyTPA-Pt(acac) films show a more balanced PL emission across the full spectral range from 1.8 to 2.9 eV. This primarily comprises distinct (1) β-phase 9,9-dioctylfluorene segment fluorescent singlet emission between 2.2 and 2.9 eV and (2) β-phase 9,9-dioctylfluorene phosphorescent triplet emission below 2.2 eV. However, the singlet emission, (1), has less clearly resolved vibronic structure than for β-phase PFO and 95F8:5PyTPA. The cyclometallated co-monomer units may be sufficiently bulky to hinder the formation of fully extended β-phase 9,9-dioctylfluorene segments leading to a broader distribution of segment extensions and environments and thereby to greater inhomogeneous broadening. The vertical displacement of the minima between groups of vibronic modes away from the zero PL line is consistent with this but could also be indicative of an overlapping, rather unstructured, emission in this range. So-called "green band" excimer emission resulting from oxidative degradation that yields keto-defects at the C-9 positions of the fluorene units does not spectrally match[29] and is, therefore, ruled out. An alternative would be emission from the PyTPA-Pt(acac) co-monomer units acting as chromophores in their own right. The spectra suggest that the displacement effect is relatively stronger at RT and also increases with PyTPA-Pt (acac) loading (see Figure S3), both of which could occur for either a state-of-order effect or PyTPA-Pt(acac) co-monomer emission. The measured emission from PyTPA-Pt(acac) co-monomer films is not, however, a good spectral match (see Figure S4b), leaving reduced film order as the most likely contributor.

The triplet phosphorescence from β-phase 95F8:5PyTPA-Pt(acac) films (shown on an expanded scale in Figure 3B) reveals a clear, relatively sharp, peak at 2.09 eV (592 nm) together with a higher energy shoulder at 2.17 eV (571 nm) and a lower energy band comprising three poorly resolved peaks centered at ~1.95 eV (638 nm). The sharp peak matches literature results for β-phase PFO triplet emission, recorded following resonant pumping of the β-phase absorption peak at 2.86 eV (434 nm) and using time gated acquisition to match the characteristically long decay time in the absence of heavy metal atoms.[30] These literature data also show two vibronic peaks in a similar spectral location to the lower two for 95F8:5PyTPA-Pt(acac) films but they do not show the higher energy shoulder or the third, higher energy vibronic

peak. It is clear, therefore, that there is an overlap between the emission from two distinct states in this spectral region. Comparison with the triplet emission from disordered poly (9,9-diethylhexylfluorene) (PF2/6)[30] suggests that the second triplet state may arise from a fraction of glassy-phase 9,9-dioctylfluorene segments in these films. This will arise when the normal rapid singlet transfer[15,21] to β-phase 9,9-dioctylfluorene segments has become hindered and/or when intersystem crossing (with consequent spatial localization on glassy chain segments) is sufficiently enhanced that it competes effectively with the singlet transfer process.

The phosphorescence from glassy-phase 95F8:5PyTPA-Pt (acac) films (shown on an expanded scale in Figure 3C) supports this surmise with the 0–0 peak at 2.17 eV (571 nm) matching the high energy shoulder in the β-phase 95F8:5PyTPA-Pt(acac) spectrum and the vibronic at 2.0 eV (622 nm) matching the highest energy component of the β-phase 95F8:5PyTPA-Pt(acac) film vibronic band. Also, as is the case for the singlet emission spectra, the triplet spectra of glassy-phase 95F8:5PyTPA-Pt(acac) are more inhomogeneously broadened to the point that the coupled vibronics are not separately identifiable. The difference spectrum in Figure 3D shows the result of subtraction of a weighted glassy-phase spectrum (Figure 3C) from the β-phase 95F8:5PyTPA-Pt(acac) film spectrum (Figure 3B) and reveals the "pure" β-phase triplet emission comprising a sharp $T_1 \rightarrow S_0$ electronic transition and a partially resolved vibronic doublet.

The emission from films, and indeed solutions, of the PyTPA-Pt(acac) co-monomer is distinct from the observed 95F8:5PyTPA-Pt(acac) film spectra (see Figure S4) further confirming that the co-monomer does not strongly influence the measured photophysics as a chromophore in its own right, as was also the case for the PyTPA co-monomer. Rather, its major influence, through the presence of the Pt heavy metal atom, is as a sensitizer for intersystem crossing within 9,9-dioctylfluorene segments. In accordance with this, both the glassy- and β-phase 95F8:5PyTPA-Pt(acac) films have a triplet emission that lies some 0.7 eV lower in energy than the singlet and that shows vibronic energies very similar to those present in the singlet, in close agreement with earlier studies of conjugated polymer triplet excitons and their S_1–T_1 gap.[31,32]

The prompt heavy metal atom sensitized phosphorescence becomes clearly visible below ~200 K and grows on further cooling, especially strongly for the glassy films (see Figure 4A and Figure S7 and S8). It is visible at 5 K for all of the β-phase PyTPA-Pt(acac) copolymer film fractions (X = 0.5, 1.0, 2.5, 5), with an intensity that depends strongly on loading (see Figure S3); some 18 times higher for 5% than 0.5%. At low loadings the β-phase 9,9-dioctylfluorene triplet phosphorescence is dominant, with the glassy-phase triplet component only growing for higher PyTPA-Pt(acac) fractions, consistent with the proposed influence of loading on film order. As the temperature rises above 200 K the prompt triplet emission falls rapidly, as expected for more-efficient triplet migration to quenching sites combined with triplet-triplet annihilation linked to this enhanced diffusion.[30,33]

As noted above, the PL spectra of glassy-phase 95F8:5PyTPA-Pt(acac) samples at low temperature show a relatively weak and largely featureless fluorescence with a more intense and structured phosphorescence. This is in contrast to the well-resolved fluorescence for the 95F8:5PyTPA-Pt(acac) β-phase films with relatively weaker phosphorescence emission. Theoretical calculations[10,34–37] suggest that this difference is due to a higher intersystem crossing rate of singlet excitons to the triplet manifold for glassy-phase compared to β-phase samples.

In Figure 4B,C the temperature dependence of representative spectral components, in particular the $S_1 \rightarrow S_0$ 0–0 fluorescence vibronic peak of β-phase PFO and the $T_1 \rightarrow S_0$ 0–0 phosphorescence vibronic peak of glassy-phase 95F8:5PyTPA-Pt(acac), is depicted on an expanded energy scale. The copolymer and PFO fluorescence spectra show, irrespective of chain conformation, a bathochromic (red) shift with decreasing temperature that approaches an asymptotic value at a characteristic temperature for which spectral diffusion saturates. In contrast, the phosphorescence spectra of 95F8:5PyTPA-Pt(acac) show two very different behaviors depending on the film microstructure. The glassy-phase film triplet emission exhibits a hypsochromic (blue) shift while the β-phase spectra remain stationary. In addition, as a result of triplet quenching, the phosphorescence spectra could not be measured at temperatures above 125 K.

In disordered organic semiconductors, the transport of excitations can be described by a hopping process among localized sites energetically distributed within an inhomogeneously broadened density of states (DOS).[38–40] The electronic coupling can be provided by either long range coulomb interactions (Förster coupling[41]), typical for singlet excitations, or short range exchange interactions (Dexter coupling[42]), for triplet excitons. Hopping theory predicts that an exciton generated within a Gaussian density of energy states distribution will relax towards the tail of the distribution by hopping among neighboring sites; this leads to a spectral diffusion with time as the mean energy of the emitting excitons evolves. The exciton path will be dominated initially by energetically downhill hops until lower lying energy sites become scarce and are thus on average a long distance away. A quasi-equilibrium, is then reached, determined by the balance between downhill jumps and thermally activated uphill jumps that allow the exciton to find an alternative

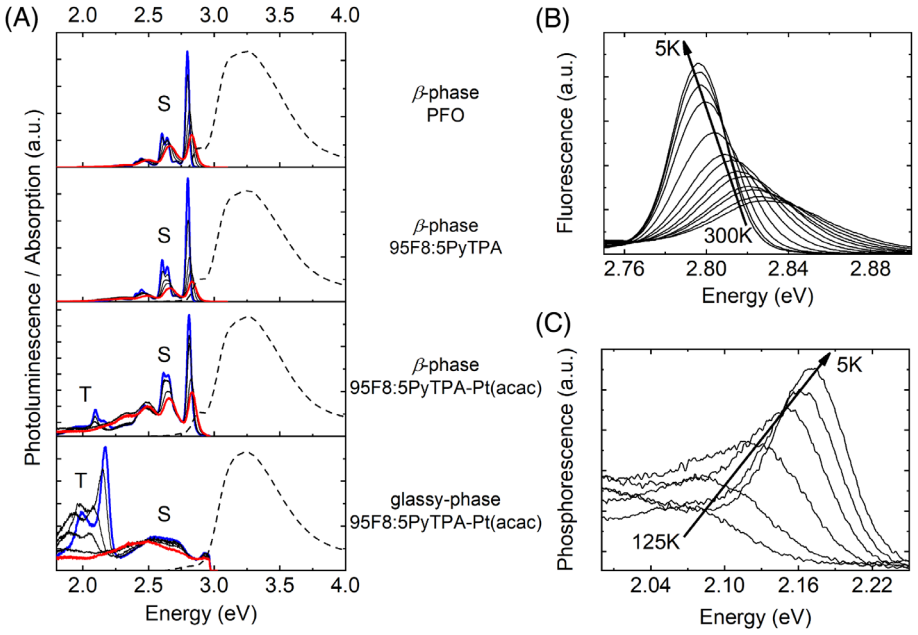

FIGURE 4 (A) Singlet (S) and triplet (T) PL spectral contributions (solid lines) at selected temperatures for (from top to bottom) β-phase PFO, 95F8:5PyTPA and 95F8:5PyTPA-Pt(acac) and glassy-phase 95F8:5PyTPA-Pt(acac) alongside their respective absorption spectra at 300 K (dashed line). The emission spectra are shown from 300 K (red lower line) to 5 K (blue upper line). (B) Spectral red-shift in the $S_1 \rightarrow S_0$ 0–0 singlet PL vibronic peak of β-phase PFO between 300 K and 5 K. (C) Spectral blue-shift in the $T_1 \rightarrow S_0$ 0–0 triplet PL vibronic peak of glassy-phase 95F8:5PyTPA-Pt(acac) between 125 K and 5 K.

path to the lower lying sites. The quasi-equilibrium energy, ε_{eqm}, is the long-time limit of the statistically weighted average energy. For a Gaussian DOS distribution, as typically found in conjugated polymer films:

$$g(\varepsilon) = \left(1/\sqrt{2\pi\sigma}\right) \exp\left(-(\varepsilon - \varepsilon_0)^2/2\sigma^2\right) \qquad (1)$$

where ε is the energy of an individual molecule, ε_0 is the energy at the center of the distribution and σ is the *standard deviation* (also known as the disorder parameter that describes the width of the distribution), $\varepsilon_{eqm} = \varepsilon_0 - \sigma^2/kT$, independent of the mode of coupling.[43] Upon lowering the temperature, the emission is thus expected to redshift before eventually becoming spectrally fixed when the time needed to reach quasi-equilibrium starts to exceed the exciton decay time.[44–47]

It is also possible to see hypsochromic (blue) spectral shifts at low temperature when the quasi-equilibrium energy can no longer be reached during the exciton decay time due to hopping activation energy considerations. This is especially the case for the short range coupling that allows triplet diffusion.[44,48] The short range Dexter process limits the number of available hopping sites relative to long range Förster transfer and if the associated energies happen to be sufficiently adverse then frustration arises, leading to exciton decay at an energy above the quasi-equilibrium energy. Illustrative spectral diffusion scenarios are depicted schematically in Figure 5.[49]

The spectral diffusion behavior observed in Figure 4 is now discussed in terms of the random walk within a Gaussian DOS model just described. First, we consider the spectral diffusion of singlet excitons. The center energy, ε_0, of the DOS is determined from the peak of the RT β-phase $S_0 \rightarrow S_1$ 0–0 absorption and its width, $\sigma(T)$, is deduced from the linewidth of the 0–0 vibrational transition of the fluorescence at different temperatures, deduced by performing a Gaussian fit to the emission spectra. The spectral shift, $\Delta\varepsilon(T)$, is then determined from the energy difference between the center of the DOS and the center of the $S_1 \rightarrow S_0$ 0–0 fluorescence emission. In Figure 6 the energy difference, $\Delta\varepsilon(T)$, normalized to $\sigma(T)$ is plotted against kT divided by $\sigma(T)$; the dashed curve is the theoretically predicted $\Delta\varepsilon(T)/\sigma(T) = -\sigma(T)/kT$ relation.

Figure 6 shows that for $kT/\sigma > 0.3$–0.4 the red-shift in the singlet fluorescence (black squares data) is in generally good agreement with the predicted dependence, albeit with a somewhat smaller than expected red-shift at the highest temperatures. At lower temperatures, however, $\Delta\varepsilon(T)/\sigma(T)$ shows clear saturation. This is a sign of the termination of spectral diffusion due to exciton decay time limitations and occurs when the transfer time needed to reach quasi-equilibrium exceeds this time. The PFO spectrum saturates at a lower value of $\Delta\varepsilon(T)/\sigma(T)$ than the 95F8:5PyTPA-Pt(acac). This is suggested to be due to the potentially shorter decay time of the 95F8:5PyTPA-Pt(acac) singlets as a result of efficient intersystem crossing to the triplet manifold, resulting from strong spin-orbit coupling of the heavy metal atom. Overall, the observed spectral diffusion of the singlet excitons is consistent with previous studies on related compounds.[44,47,49]

Repeating the analysis for the triplet phosphorescence spectra recorded for the two phases of 95F8:5PyTPA-Pt(acac) leads to the red circles data in Figure 6. For the β-phase

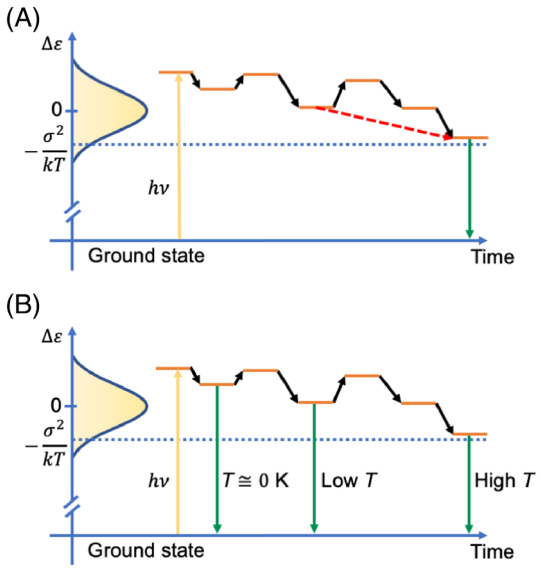

FIGURE 5 Schematic illustration of spectral diffusion processes for singlets and triplets. Gaussian DOS drawn with $\varepsilon_0 = 0$. Over time the excitons explore the distribution of states in space and energy. (A) Directly photoexcited singlet excitons hop from site to site (solid black arrows), sometimes requiring thermal activation (upward pointing arrows). At sufficiently high temperatures, the quasi-equilibrium energy is readily reached and emission takes place from there. At low temperatures, activated jumps away from some intermediate sites are frozen out but the long range Förster transfer helps keep lower energy sites accessible (dotted red arrow) so that the quasi-equilibrium energy can still be reached. Eventually the exciton decay time limits the transfer process and the quasi-equilibrium energy is no longer reached, leading to a saturation of the red-shift. (B) for triplets, generated following intersystem crossing from photoexcited singlets, the absence of long range Förster transfer means that whilst at sufficiently high temperatures triplet excitons do reach the quasi-equilibrium energy, at lower temperatures when activated jumps away from some intermediate sites are no longer possible the exciton becomes trapped and decays at that site. This can lead to a blue-shift with decreasing temperature. Redrawn from reference.[49]

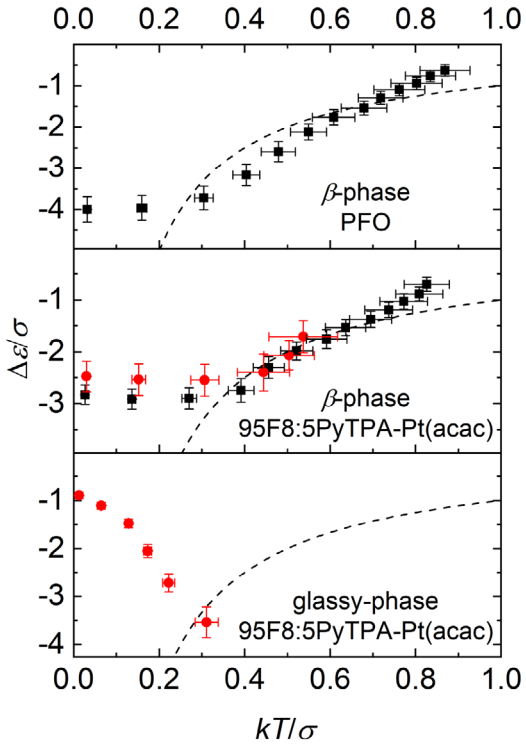

FIGURE 6 Energy difference $\Delta\varepsilon$ between the center of the DOS and the centers of the $S_1 \rightarrow S_0$ 0–0 fluorescence (black squares) and $T_1 \rightarrow S_0$ 0–0 phosphorescence (red circles) peaks, normalized to DOS width σ and plotted versus kT/σ. data are shown for β-phase PFO and 95F8:5PyTPA-Pt(acac) and for glassy-phase 95F8:5PyTPA-Pt(acac). The dashed curve is the theoretically predicted $\Delta\varepsilon(T)/\sigma(T) = -\sigma(T)/kT$ dependence.

samples the glassy-phase component in their spectra, that remains relatively constant with temperature, is first subtracted before the fitting is undertaken. The center of the DOS of the triplet states is selected by considering the mirror symmetry between absorption and emission and the disorder parameter, σ, is deduced from the linewidth of the $T_1 \rightarrow S_0$ 0–0 emission. Due to triplet quenching, suitable data could not be collected above 125 K and, therefore, the triplet exciton behavior was studied only for lower temperature spectra. The two phases of the copolymer show very different behavior. The β-phase triplets behave in a similar way to the corresponding singlets, with saturation for $kT/\sigma < 0.4$. Conversely, for the glassy-phase a strong hypsochromic (blue) shift is observed for $kT/\sigma < 0.3$. This difference in behavior is significant and offers an important insight into the role that microstructure plays in the triplet exciton transfer occurring within a single material.

The motion of triplet excitons proceeds by short range exchange interactions which decrease exponentially with coupling distance.[42] Exchange interactions require orbital spatial overlap, further restricting the number of target sites for transfer. Frustration can then occur when all nearest neighbors have a higher energy which cannot be overcome with the available thermal energy and the triplet becomes trapped in a local energy minimum from which emission occurs. As illustrated schematically in Figure 5B the local minima tend to lie at increasingly higher energies for lower temperatures, resulting in the hypsochromic shift observed in Figure 4C and 6 (bottom panel). This contrasts with the Förster transfer of singlets that has an algebraic dependence on coupling distance and does not require spatial overlap of wavefunctions.[41] As a consequence, transfer between sites that are located further apart is supported, generating a larger number of targets for transfer to and thereby allowing diffusion over large distances without the need for thermal activation;

the probability of reaching a site at an accessible energy increases when longer range hops are possible.

The hypsochromic shift seen for triplets in glassy-phase 95F8:5PyTPA-Pt(acac) is thus in good agreement with theory and consistent with published experiments for exciton transfer via short range exchange interactions in other conjugated polymers.[45–47] The triplet spectra of the β-phase samples, however, show behavior which is similar to that expected for singlets, with a low temperature saturation in the spectral dispersion. Whilst it is clear that the DOS variances, σ^2, for the glassy- and β-phase chain segments differ (emission linewidth larger for more disordered glassy-phase),[21,50] this is accounted for in Figure 6 by normalizing the data to units of σ. The lack of frustration in the more ordered β-phase cannot then be due to a smaller disorder parameter. Instead, the difference stems from a key change in microstructure, namely the increased conjugation length of the β-phase chain segments. These rigid, planar segments embedded within a glassy matrix, comprise minima in the triplet and singlet energy spaces and will tend to capture both exciton types from neighboring glassy-phase chain segments. Then, in agreement with Monte Carlo simulations,[44] their chain-extended structure allows the triplets to readily migrate along their length, increasing the number of accessible neighbors and removing the cause of the hypsochromic shift seen for glassy-phase samples. Similar behavior has been reported for another highly-planar conjugated polymer, namely methyl-substituted ladder-type poly(p-phenylene) (MeLPPP).[49] These results demonstrate that triplet diffusion in the platinum containing polyfluorene copolymer 95F8:5PyTPA-Pt(acac) can be greatly affected by the film microstructure and while frustration is observed for the glassy-phase, it can be avoided by generating chain-extended β-phase conformation segments. To our knowledge, this represents the first demonstration of the use of a controlled change in molecular conformation to control the triplet diffusion properties in a material.

3 | CONCLUSIONS

Novel fluorene-based copolymers (Figure 1) have been synthesized and their photophysical properties investigated in depth at both RT and as a function of temperature down to 5 K. Incorporation of PyTPA and PyTPA-Pt(acac) co-monomer units at fractions between 0.5% and 5% into an otherwise (9,9-dioctylfluorene) backbone yields two families of copolymers with and without the presence of heavy Pt atoms. For this range of co-monomer fractions the β-phase conformation can still be readily generated in the (9,9-dioctylfluorene) segments (Figure 2), allowing the influence of conformation to be carefully studied, with homopolymer poly(9,9-dioctylfluorene) providing a suitable reference. At RT (Figure 2) the PyTPA co-monomers have little influence, with some monomer-centered emission observed for 95F8:5PyTPA glassy conformation films but very little for the β-phase. The PyTPA-Pt(acac) co-monomer has a bigger impact, mainly via its sensitization of intersystem crossing which reduces singlet PL emission. At low temperature (5 K), the PyTPA-Pt(acac) co-monomer films show direct $T_1 \rightarrow S_0$ radiative decay from 9,9-dioctylfluorene-segment-based triplet states whilst the PyTPA co-monomers again have little effect on the photophysics, especially for β-phase samples (Figure 3) which closely mirror the PL behavior of PFO. The glassy-phase 95F8:5PyTPA-Pt(acac) spectra are most perturbed with the PL dominated by $T_1 \rightarrow S_0$ emission, albeit with an overall lower emission yield than for the β-phase samples.

The spectral diffusion for both singlet and triplet excitons has been investigated in detail for β-phase PFO and glassy- and β-phase 95F8:5PyTPA-Pt(acac) copolymer films, using experimental PL spectra recorded as a function of temperature between 5 and 300 K (Figure 4) and a Gaussian disorder model analysis (Figures 5 and 6). The theoretically predicted bathochromic (red) shift behavior is seen for singlet exciton diffusion in PFO and 95F8:5PyTPA-Pt(acac) β-phase samples down to temperatures at which the diffusion finally freezes out. For the triplets, however, the glassy- and β-phase 95F8:5PyTPA-Pt(acac) films show different behaviors. In the former case, the triplet exciton emission spectra show a hypsochromic (blue) shift on cooling whilst in the latter case the behavior is similar to that of the singlets with spectral saturation observed at low temperature rather than a blue-shift.

These observations provide insight into the triplet exciton transfer in more- or less-disordered conjugated polymer films. The glassy films possess a shorter ensemble average conjugation length whereas the β-phase films combine a fraction of chain-extended segments embedded within a glassy matrix. It is found in the glassy-phase samples with shorter conjugation lengths (representative of more-disordered polymers) that the triplet exciton relaxation becomes frustrated at low temperature due to a freezing out of the thermally activated hops required to move from one conjugated segment to another. In contrast, for films containing β-phase chain segments, with increased conjugation lengths (representative of less-disordered polymers), this frustration is lifted as more hopping sites remain accessible through intra-segment motion. The triplet can consequently explore a larger number of potential acceptor sites yielding a non-thermally-activated triplet transfer.

This work demonstrates the controlled use of changes in molecular conformation to successfully optimize the

triplet diffusion properties of a fluorene-based conjugated copolymer. Future work will study how broadly such conformation control can be applied to other material systems for device applications. For example, triplet transporting materials have been used in solar cells and for triplet up-conversion, whilst triplet diffusion is known to be detrimental to phosphorescent LEDs in the presence of quenching sites.

4 | EXPERIMENTAL SECTION

4.1 | Materials

The PFO homopolymer was purchased from 1-Material Inc. (weight-average molecular weight (M_w) = 55 × 10^3 g mol^{-1} and polydispersity index (PDI) = 2.5) and used as received. The novel copolymers were synthesized in Nanjing Tech via Suzuki coupling and subjected to standard analytical characterization, comprising ^{1}H NMR, elemental analysis, energy-dispersive X-ray spectroscopy (EDS), gel permeation chromatography, thermogravimetric analysis, differential scanning calorimetry and cyclic voltammetry (see Supporting Information for details). These results confirm successful synthesis of the target materials and give useful insight into the ensuing physical properties. From EDS, the platinum element weight ratios of the Pt-containing copolymers (100-X)F8:XPyTPA-Pt(acac) (X = 0.5, 1, 2.5 and 5) were measured to be 0.22, 0.46, 1.20, and 2.21 wt%, which are very close to the theoretical values of 0.25, 0.50, 1.24, and 2.49 wt%, respectively. The results indicate the cyclometalated Pt-containing fragments were successfully incorporated into the 9,9-dioctylfluorene backbones according to the different molar feed ratios. The 95F8:5PyTPA-Pt(acac) copolymer had M_w = 74 × 10^3 g mol^{-1} with PDI = 2.31 and the 95F8:5PyTPA copolymer had M_w = 66 × 10^3 g mol^{-1} with PDI = 1.94.

4.2 | Film preparation

For optical measurements, thin films were spin coated at 2000 rpm from 10 mg ml^{-1} toluene solutions onto quartz (Spectrosil B) substrates in a nitrogen-filled glove box. A Dektak Systems surface profilometer was used to measure the resulting film thickness, typically ∼70 nm. For the preparation of glassy-phase films both solution vials and substrates were placed on a hot plate at 100°C for 5 min immediately prior to spin coating. For β-phase samples solvent vapor annealing of glassy films was employed. This was done via exposure to toluene vapor at RT for 12 h with film swelling generating the mechanical stress that drives planarization of a fraction of the polymer chains.[22,26,27] We follow the convention in the literature that samples containing such a fraction of β-phase chains in an otherwise glassy film are called β-phase samples, irrespective of the specific fraction. Low temperature spectral data are not reported for glassy-phase films of PFO and the PyTPA copolymer as it was found that they were not stable during thermal cycling against partial formation of β-phase segments; a phenomenon already known in the literature for PFO.[21]

4.3 | UV–Vis spectroscopy

Optical absorption spectra were measured with a Perkin-Elmer Lambda 1050 UV/Vis/NIR spectrophotometer equipped with a Perkin-Elmer 100 mm integrating sphere accessory.

4.4 | Photoluminescence spectroscopy

Temperature dependent PL spectra were measured with samples mounted on *xyz* piezo positioners in a closed cycle AttoDRY800 cryostat pumped to a residual pressure of ∼10^{-6} mbar and cycled between RT and 5 K. PL excitation was provided by a 76 MHz Coherent Mira 900 Titanium-Sapphire laser producing ∼100 fs pulses, with the repetition rate down-selected using a Coherent pulse picker to lie in the range 0.76–3.8 MHz. The excitation energy of ∼3.15 eV (394 nm), suitably matched to the polymer optical gaps, was obtained by frequency doubling the laser using an INRAD 5–050 Ultrafast Harmonic Generation System. A single mode optical fiber routed the excitation light to the PL setup and the excitation power was adjusted using a neutral density filter. The laser light was focused onto a roughly 1 μm diameter spot on the sample by a Mitutoyo Apo objective (NA = 0.7, 100× magnification) which was also used to collect the PL. A Semrock Di02-R405-25x36 dichroic mirror and a Semrock BLP01-405R-25 filter were placed in the emission path to reject residual excitation light and transmit only the desired PL signal. A 0.5 m Andor spectrometer (spectral resolution ∼0.07 nm) coupled to a thermoelectrically cooled iDus 420 charge coupled device detector was used to scan and record the PL emission spectra. The combination of the used repetition rate and detection mode selects prompt PL. The PL spectra in Figure 2A and S2 were recorded in reflection geometry using a Jobin Yvon Horiba Fluoromax-3 spectrofluorometer (3.2 eV excitation) in ambient air.

ACKNOWLEDGMENTS

Nikol T. Lambeva and Donal D. C. Bradley acknowledge studentship funding from the UK Engineering and

Physical Sciences Research Council [grant number 1734270] together with equipment funding from Oxford University. Donal D. C. Bradley further acknowledges support from the King Abdullah University of Science and Technology. Youtian Tao and Donal D. C. Bradley also acknowledge support from the Jiangsu Province Double Creation Team funding program.

DATA AVAILABILITY STATEMENT

The data that support the findings of this study are available from the corresponding author upon reasonable request.

ORCID

Nikol T. Lambeva https://orcid.org/0000-0002-9003-1366
Xuyu Gao https://orcid.org/0000-0003-4116-3028
Youtian Tao https://orcid.org/0000-0002-3133-4981

REFERENCES

[1] S. Reineke, F. Lindner, G. Schwartz, N. Seidler, K. Walzer, B. Lüssem, K. Leo, *Nature* **2009**, *459*, 234.
[2] G. Schwartz, S. Reineke, T. C. Rosenow, K. Walzer, K. Leo, *Adv. Funct. Mater.* **2009**, *19*, 1319.
[3] Y. Sun, N. C. Giebink, H. Kanno, B. Ma, M. E. Thompson, S. R. Forrest, *Nature* **2006**, *440*, 908.
[4] M. Lehnhardt, T. Riedl, T. Rabe, W. Kowalsky, *Org. Electron.* **2011**, *12*, 486.
[5] Y. Luo, H. Aziz, *Adv. Funct. Mater.* **2010**, *20*, 1285.
[6] M. Lebental, H. Choukri, S. Chénais, S. Forget, A. Siove, B. Geffroy, E. Tutiš, *Phys. Rev. B - Condens. Matter Mater. Phys.* **2009**, *79*, 1.
[7] S. Baluschev, P. E. Keivanidis, G. Wegner, J. Jacob, A. C. Grimsdale, K. Müllen, T. Miteva, A. Yasuda, G. Nelles, *Appl. Phys. Lett.* **2005**, *86*, 1.
[8] F. Laquai, G. Wegner, C. Im, A. Büsing, S. Heun, *J. Chem. Phys.* **2005**, *123*, 074902.
[9] A. Monguzzi, R. Tubino, F. Meinardi, *Phys. Rev. B - Condens. Matter Mater. Phys.* **2008**, *77*, 3.
[10] L. Qin, X. Liu, X. Zhang, J. Yu, L. Yang, F. Zhao, M. Huang, K. Wang, X. Wu, Y. Li, H. Chen, K. Wang, J. Xia, X. Lu, F. Gao, Y. Yi, H. Huang, *Angew. Chemie - Int. Ed.* **2020**, *59*, 15043.
[11] Y. Yang, J. Wei, R. Li, Z. Zhang, *ChemistrySelect* **2022**, *7*, e202201647.
[12] J. G. Yang, X. F. Song, G. Cheng, S. Wu, X. Feng, G. Cui, W. P. To, X. Chang, Y. Chen, C. M. Che, C. Yang, K. Li, *ACS Appl. Mater. Interfaces* **2022**, *14*, 13539.
[13] M. Ariu, D. G. Lidzey, M. Sims, A. J. Cadby, P. A. Lane, D. D. C. Bradley, *J. Phys. Condens. Matter* **2002**, *14*, 9975.
[14] M. Ariu, M. Sims, M. D. Rahn, J. Hill, A. M. Fox, D. G. Lidzey, M. Oda, J. Cabanillas-Gonzalez, D. D. C. Bradley, *Phys. Rev. B - Condens. Matter Mater. Phys.* **2003**, *67*, 1.
[15] A. Perevedentsev, N. Chander, J. S. Kim, D. D. C. Bradley, *J. Polym. Sci. Part B: Polym. Phys.* **2016**, *1995*, 54.
[16] I. Hamilton, N. Chander, N. J. Cheetham, M. Suh, M. Dyson, X. Wang, P. N. Stavrinou, M. Cass, D. D. C. Bradley, J. S. Kim, *ACS Appl. Mater. Interfaces* **2018**, *10*, 11070.
[17] B. Wang, H. Ye, M. Riede, D. D. C. Bradley, *ACS Appl. Mater. Interfaces* **2021**, *13*, 2919.
[18] W. Chunwaschirasiri, B. Tanto, D. L. Huber, M. J. Winokur, *Phys. Rev. Lett.* **2005**, *94*, 3.
[19] M. Grell, D. D. C. Bradley, X. Long, T. Chamberlain, M. Inbasekaran, E. P. Woo, M. Soliman, *Acta Polym.* **1998**, *49*, 439.
[20] M. Grell, D. D. C. Bradley, G. Ungar, J. Hill, K. S. Whitehead, *Macromolecules* **1999**, *32*, 5810.
[21] A. J. Cadby, P. A. Lane, H. Mellor, S. J. Martin, M. Grell, C. Giebeler, D. D. C. Bradley, M. Wohlgenannt, C. An, Z. V. Vardeny, *Phys. Rev. B - Condens. Matter Mater. Phys.* **2000**, *62*, 15604.
[22] A. L. T. Khan, P. Sreearunothai, L. M. Herz, M. J. Banach, A. Köhler, *Phys. Rev. B - Condens. Matter Mater. Phys.* **2004**, *69*, 1.
[23] J. Peet, E. Brocker, Y. Xu, G. C. Bazan, *Adv. Mater.* **2008**, *1882*, 20.
[24] H. H. Lu, C. Y. Liu, C. H. Chang, S. A. Chen, *Adv. Mater.* **2007**, *19*, 2574.
[25] M. C. Chen, W. C. Hung, A. C. Su, S. H. Chen, S. A. Chen, *J. Phys. Chem. B* **2009**, *113*, 11124.
[26] M. E. Caruso, M. Anni, *Phys. Rev. B - Condens. Matter Mater. Phys.* **2007**, *76*, 1.
[27] G. Ryu, P. N. Stavrinou, D. D. C. Bradley, *Adv. Funct. Mater.* **2009**, *19*, 3237.
[28] A. J. Sandee, C. K. Williams, N. R. Evans, J. E. Davies, C. E. Boothby, A. Köhler, R. H. Friend, A. B. Holmes, *J. Am. Chem. Soc.* **2004**, *126*, 7041.
[29] M. Sims, D. D. C. Bradley, M. Ariu, M. Koeberg, A. Asimakis, M. Grell, D. G. Lidzey, *Adv. Funct. Mater.* **2004**, *14*, 765.
[30] C. Rothe, S. M. King, F. Dias, A. P. Monkman, *Phys. Rev. B - Condens. Matter Mater. Phys.* **2004**, *70*, 1.
[31] A. Köhler, J. S. Wilson, R. H. Friend, M. K. Al-Suti, M. S. Khan, A. Gerhard, H. Bässler, *J. Chem. Phys.* **2002**, *116*, 9457.
[32] A. Köhler, D. Beljonne, *Adv. Funct. Mater.* **2004**, *14*, 11.
[33] D. Hertel, S. Setayesh, H. G. Nothofer, U. Scherf, K. Müllen, H. Bässler, *Adv. Mater.* **2001**, *13*, 65.
[34] D. Beljonne, Z. Shuai, G. Pourtois, J. L. Bredas, *J. Phys. Chem. A* **2001**, *105*, 3899.
[35] A. Hayer, A. L. T. Khan, R. H. Friend, A. Köhler, *Phys. Rev. B - Condens. Matter Mater. Phys.* **2005**, *71*, 1.
[36] K. Schmidt, S. Brovelli, V. Coropceanu, D. Beljonne, J. Cornil, C. Bazzini, T. Caronna, R. Tubino, F. Meinardi, Z. Shuai, J. L. Brédas, *J. Phys. Chem. A* **2007**, *111*, 10490.
[37] Y. Tamai, H. Ohkita, H. Benten, S. Ito, *Chem. Mater.* **2014**, *26*, 2733.
[38] H. Bässler, A. Köhler, *Top. Curr. Chem.* **2012**, *312*, 1.
[39] W. F. Pasveer, J. Cottaar, C. Tanase, R. Coehoorn, P. A. Bobbert, P. W. M. Blom, M. De Leeuw, M. A. J. Michels, *Phys. Rev. Lett.* **2005**, *94*, 1.
[40] S. L. M. Van Mensfoort, S. I. E. Vulto, R. A. J. Janssen, R. Coehoorn, *Phys. Rev. B - Condens. Matter Mater. Phys.* **2008**, *78*, 1.
[41] T. Förster, *Discuss. Faraday Soc.* **1959**, *27*, 7.
[42] D. L. Dexter, *J. Chem. Phys.* **1953**, *21*, 836.
[43] B. Movaghar, M. Grünewald, B. Ries, H. Bassler, D. Würtz, *Phys. Rev. B - Condens. Matter Mater. Phys.* **1986**, *33*, 5545.
[44] S. Athanasopoulos, S. T. Hoffmann, H. Bässler, A. Köhler, D. Beljonne, *J. Phys. Chem. Lett.* **2013**, *4*, 1694.

[45] L. S. Devi, M. K. Al-Suti, C. Dosche, M. S. Khan, R. H. Friend, A. Köhler, *Phys. Rev. B - Condens. Matter Mater. Phys.* **2008**, *78*, 1.
[46] I. I. Fishchuk, A. Kadashchuk, L. Sudha Devi, P. Heremans, H. Bässler, A. Köhler, *Phys. Rev. B - Condens. Matter Mater. Phys.* **2008**, *78*, 1.
[47] S. T. Hoffmann, E. Scheler, J. M. Koenen, M. Forster, U. Scherf, P. Strohriegl, H. Bässler, A. Köhler, *Phys. Rev. B - Condens. Matter Mater. Phys.* **2010**, *81*, 1. https://doi.org/10.1103/PhysRevB.81.165208
[48] A. Köhler, H. Bässler, *Electronic Processes in Organic Semiconductors*, Wiley-VCH Verlag GmbH, Weinheim, Germany **2015**.
[49] S. T. Hoffmann, H. Bässler, J. M. Koenen, M. Forster, U. Scherf, E. Scheler, P. Strohriegl, A. Köhler, *Phys. Rev. B - Condens. Matter Mater. Phys.* **2010**, *81*, 1. https://doi.org/10.1103/PhysRevB.81.115103
[50] M. J. Winokur, J. Slinker, D. L. Huber, *Phys. Rev. B - Condens. Matter Mater. Phys.* **2003**, *67*, 1.

SUPPORTING INFORMATION

Additional supporting information can be found online in the Supporting Information section at the end of this article.

How to cite this article: N. T. Lambeva, C. C. Mullen, X. Gao, Q. Wu, R. A. Taylor, Y. Tao, D. D. C. Bradley, *J. Polym. Sci.* **2023**, *61*(1), 83. https://doi.org/10.1002/pol.20220366